Intra-cortical propagation of EEG alpha oscillations

Rikkert Hindriks[1,*], Michel J.A.M. van Putten[2,3], Gustavo Deco[1,4]

1. Center for Brain and Cognition, Computational Neuroscience Group, Department of Information and Communication Technologies, Universitat Pompeu Fabra, Roc Boronat 138, Barcelona, 08018, Spain

2. Department of Clinical Neurophysiology, MIRA-Institute for Biomedical Technology and Technical Medicine, University of Twente, 7500 AE Enschede, The Netherlands

3. Department of Neurology and Clinical Neurophysiology, Medisch Spectrum Twente, Enschede, The Netherlands

4. Instituci Catalana de la Recerca i Estudis Avanats (ICREA), Universitat Pompeu Fabra, Passeig Llus Companys 23, Barcelona, 08010, Spain

* Corresponding author: Rikkert.Hindriks@upf.edu

Abstract

The most salient feature of spontaneous human brain activity as recorded with electroencephalography (EEG) are high-voltage rhythmic fluctuations around 10 Hz. These *alpha oscillations* have been reported to propagate over the scalp with velocities in the range of 5 - 15 m/s. Since these velocities are in the range of action potential velocities through cortico-cortical axons, it has been hypothesized that the observed scalp waves reflect cortico-cortically mediated propagation of cortical oscillations. The reported scalp velocities however, appear to be inconsistent with those estimated from local field potential recordings in dogs, which are < 1 m/s and agree with the propagation velocity of action potentials in intra-cortical axons. In this study, we resolve these diverging findings using a combination of EEG data-analysis and biophysical modeling. In particular, we demonstrate that the observed scalp velocities can be accounted for by slow traveling oscillations, which provides support for the claim that spatial propagation of alpha oscillations is mediated by intra-cortical axons.

1 Introduction

Alpha oscillations can be recorded from mammalian neocortex, particularly during wakeful detachment from the environment. Although initially regarded as "idling rhythms", recent observations of their ability to modulate sensory awareness and reaction times suggests a central role in perceptual and motor function (Klimesch et al., 2007; Dijk et al., 2008). In addition, recent experiments have provided evidence that alpha oscillations are intimately linked to early sensory-evoked potentials (Makeig et al., 2002; Nikulin and Brismar, 2006; Mazaheri and Jensen, 2008). Besides their involvement in perceptual processing, experiments in human and macaque have demonstrated their involvement in regulating attention, working memory processes, and provide selective inhibition of task-irrelevant networks (Klimesch, 1999; Jensen et al., 2002; Klimesch et al., 2007; Mo et al., 2011).

In contrast to the dynamics of localized alpha sources, which have been investigated in numerous studies, spatial propagation of alpha oscillations has received considerably less attention. Human EEG studies have shown however, that resting-state as well as stimulus-induced alpha oscillations travel over the scalp (Burkitt et al., 2000; Nunez et al., 2001; Ito et al., 2005; Klimesch et al., 2007) and that their wave properties correlate with reaction times (Fellinger et al., 2012; Patten et al., 2012), indicating their potential functional relevance. These observations however, pertain to scalp signals and the properties of the underlying waves on the cortical sheet are unclear at present. Because scalp velocities lie in the range 5 - 15 m/s, it has been suggested that alpha scalp waves are propagate through cortico-cortical axons, which have conduction velocities in this range (Kandel et al., 2000). The resuling long wavelengths, combined with predominant propagation along the medial axis have been proposed to endow alpha oscillations with suitable properties to mediate top-down and bottom-up interactions between occipital and frontal networks (Burkitt et al., 2000; Nunez et al., 2001; Ito et al., 2005; Klimesch et al., 2007;

Patten et al., 2012).

The reported velocities obtained from scalp EEG recordings seem inconsistent with those obtained from invasive recordings, which are about an order of magnitude lower. Local field potential (LFP) recordings in dogs visual cortex lead to estimates of about 0.3 m/s (Lopes Da Silva et al., 1980). More recently, electrocorticographic (EcoG) recordings in human subjects have led to estimates of propagation velocities in the range 0.7-2.1 m/s (Bahramisharif et al., 2013). Intriguingly, the authors observed gamma bursts propagating with the same velocity and riding on the troughs of the propagating alpha oscillations. The slow propagation velocities obtained from invasive recordings are consistent with voltage-sensitive dye (VSD), optical imaging, and local field potential recordings of other kinds of neocortical activity, which lead to propagation velocities < 1 m/s suggesting mediation through intra-cortical instead of cortico-cortical axons (Ermentrout and Kleinfeld, 2001; Han et al., 2008; Wu et al., 2008; Zheng and Yao, 2012), Besides the inconsistency in reported traveling velocites between scalp EEG and invasive recordings, annother difference is that in the latter, systematic propagation of single-cycle oscillations is reported, while the former report propagation of single-cycle oscillations only in a fraction of cycles (Ito et al., 2005; Patten et al., 2012).

In this study we resolve these issues by combining a method to extract wave-activity from scalp EEG recordings with current source density simulations. The proposed method shows that single-cycle alpha oscillations propagate over the scalp, consistent with the observations of VSD and LFP studies. Furthermore, the simulations show that intra-cortical propagation of alpha oscillations through cortical sulci or gyri can account for the observed scalp velocities. We further varify the intra-cortical hypothesis of alpha propagation by formulating and verifying a number of predictions on the behavior of alpha scalp waves. Importantly, the wavelengths implied by the intra-cortical hypothesis are estimated to be in the order of several centimeters, much smaller than predicted

by the cortico-cortical hypothesis, provoking a re-examination of the notion of alpha-mediated long-range interactions.

2 Materials and Methods

Cortico-cortical versus intra-cortical propagation

Figure 1A illustrates the cortico-cortical and intra-cortical hypothesis on alpha propagation. According to the cortico-cortical hypothesis, electric potential waves on the scalp reflect cortical waves with similar velocity (5 - 15 m/s) that are mediated through cortico-cortical axons, which are known to have conduction velocities in this range (Kandel et al., 2000). According to the intra-cortical hypothesis, advocated in this study, the traveling scalp waves result from relatively localized and slowly propagating cortical oscillations, that are mediated by slowly conducting and short-range intra-cortical axons. To see how slow and local intra-cortically propagating oscillations can give rise to fast and global traveling waves and formulate predictions, we use a simulation to illustrate the predictions that follow from the hypothesis that cortical alpha oscillations propagate through intra-cortical axons. For the simulation we used the Montreal Neurological Institute (MNI) template of the human cortical sheet taken from the Statistical Parametric Mapping (SPM) software (http://www.fil.ion.ucl.ac.uk/spm/software/spm8). The cortical sheet was used to simulate intra-cortically traveling alpha oscillations (Section 2.3), from which scalp potentials were calculated using a 3-shell volume conductor model (Section 2.2). The simulation is shown in Figure 1B.

First note that the cortical traveling wave indeed gives rise to a traveling wave on the scalp (in this simulation, along the lateral axis from left to right). Furthermore, both the positive and negative potentials traverse the scalp during one alpha-cycle, which explains their high velocity and hence their long spatial wavelengths. Furthermore, if the frequency of the alpha oscillations

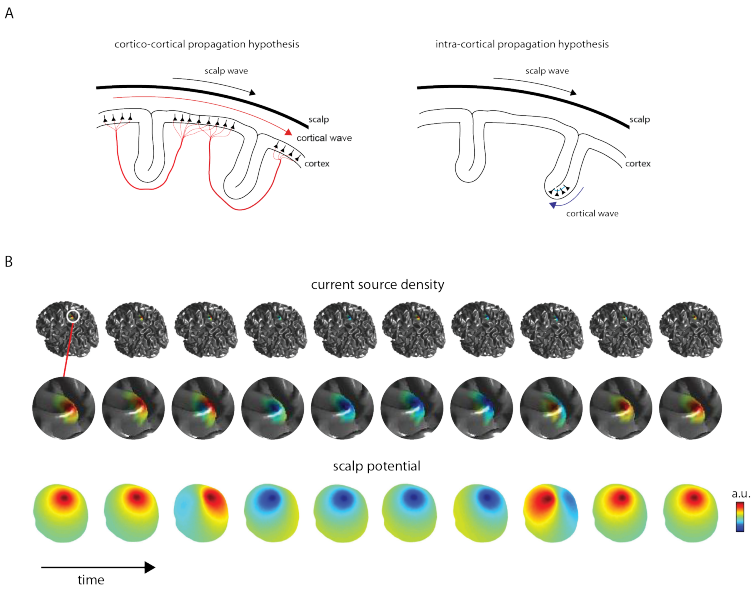

Figure 1: Spatial propagation of alpha oscillations. A. Schematic illustration of the cortico-cortical (left) and intra-cortical (right) hypothesis of propagation of cortical alpha oscillations. According to the cortico-cortical hypothesis, alpha oscillations propagate through neocortex via cortico-cortical axons (red curves) which leads to fast propagation and long-wavelengths. According to the intra-cortical hypothesis, alpha oscillations propagate through intra-cortical axons (blue curves) which leads to slow propagation and small wavelengths. In both cases, conduction of the generated electric fields through cortex, cerebrospinal fluid, skull, and scalp leads to traveling waves on the scalp, which are recorded with EEG. B. Top two rows: Current source densities (CSD) of a simulated alpha oscillation traveling over a cortical gyrus. The frames are taken every 10 ms and span one alpha cycle (the alpha peak-frequency was set to 9 Hz). The propagation velocity is chosen in the range of propagation velocities of action potentials in intra-cortical axons (< 1 m/s), giving rise to a wavelength in the order of centimeters. Bottom row: Induced scalp electric potential maps. The scalp potential behaves like a fast-propagating traveling wave along the lateral axis with long wavelength. Note that traveling direction reflects the local geometry of the underlying activated cortex.

increases, the positive and negative potentials still traverse the scalp during a single alpha-cycle. The intra-cortical hypothesis thus predicts that alpha peak-frequency correlates with scalp velocity. Second, alpha scalp waves have consistently been reported to travel along the medial axis and to be in anti-phase between occipital and frontal electrodes (Burkitt et al., 2000; Nunez et al., 2001; Ito et al., 2005; Klimesch et al., 2007). This has been explained under the cortico-cortical hypothesis by assuming boundary conditions on the cortical sheet (Nunez et al., 2001), which could lead to standing waves. In contrast, according to the intra-cortical hypothesis, the phase difference of exactly half an oscillation cycle is due to the fact that the scalp potential field resulting from a localized cortical activation has a dipolar shape. In Figure 1B, for example, the oscillations recorded from electrodes overlying left and right temporal cortex are in anti-phase. Moreover, the direction of propagation reflects the local orientation of activated cortical tissue. In Section 2.7 we provide a mathematical derivation of these properties and a number of predictions of the behavior of alpha scalp waves under the intra-cortical hypothesis of alpha propagation.

2.1 EEG recordings and pre-processing

We used EEG recordings collected from the Neurocenter EEG database from the Medisch Spectrum Twente, Enschede, The Netherlands, which consist of paired eyes-closed resting-state and propofol-induced general anesthesia recordings of 21 patients that underwent surgery for carotid endarterectomy. In all these patients, the EEG was recorded as a standard procedure to determine if temporary shunting is needed (van Putten et al., 2004). We manually selected those patients whose EEG displayed clear alpha activity in both the resting-state and anesthesia condition. This resulted in the selection of continuous EEG epochs of 14 subjects with durations varying between 41 and 153 seconds. In this study we only use the resting-state data. All recording were performed using a Brainlab EEG recording system (OSG, bvba, Belgium) comprising 21 silverchloride cup electrodes placed on the scalp according to the international 10-20 system. Average-reference mon-

tage was used to approximate an inactive reference. The time-series were down-sampled to 250 Hz and bandpass filtered using a 4-th order Butterworth filter with bandwidth ±2 Hz around the subjects' individual alpha peak-frequencies.

In addition, we recorded five-minute eyes-closed resting-state EEG data from two subjects using a 64-channel full-band amplifier (Refa, TMSi, Oldenzaal, Netherlands) against a common average. Electrode impedances were kept below 5 kOhm. The ground electrode was placed between electrode positions Fz and FPz. The signals were low-pass filtered using an anti-aliasing filter with a cut-off frequency of 550 Hz. The time-series were subsequently down-sampled to 256 Hz and bandpass filtered using a 4-th order Butterworth filter with bandwidth ±1 Hz around the subjects' individual alpha peak-frequencies.

2.2 Current source density simulations

To assess if the intra-cortical hypothesis can explain the reported properties of alpha scalp waves, we model the current source density (CSD) $s(x, y, t)$ on a square piece of cortex as a traveling wave with temporal frequency f_α in the alpha range (7 - 13 Hz), propagation speed v in the range of that recorded in intra-cortical axons (0.1 - 1 m/s) (Kandel et al., 2000), and amplitude A_s in the range measured during visually evoked potentials in unanesthetized monkeys (50 - 250 nA/mm^2) (Hamalainen et al., 1993). MEG recordings suggest that the CSD of occipital alpha oscillations in humans are in the same range and that the associated dipole moments are generated by sources with a spatial extent of about 3 cm^2 (Hamalainen et al., 1993; **?**; Nunez et al., 2001). We thus assume that the characteristic length constant γ_1 in the direction perpendicular to the traveling direction lies in the range 1 - 2 cm, with a nominal value of 1.5 cm. In the absence of measurements, we assume that the characteristic length constant γ_2 in the direction parallel to the traveling direction lies in the range 1 - 10 cm, with a nominal value of 5 cm.

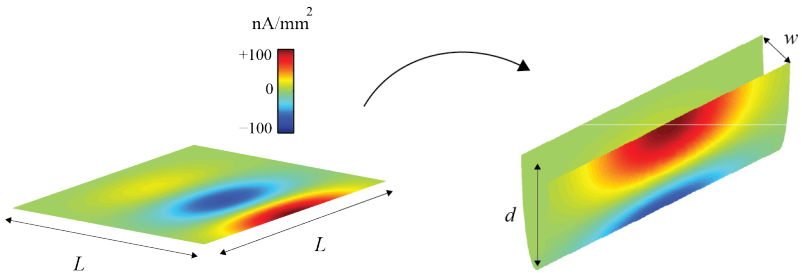

Figure 2: Parametrization of cortical sulcus. Shown is a piece of modeled cortex of extension L^2 cm^2 which is mapped into three-dimensional space by an approximately isometric and area-preserving map. This results in a sulcus with width w cm, depth d cm, and length L cm. A snapshot of the simulated CSD dynamics is color-coded.

The cortical square is subsequently curved by an area-preserving and approximately isometric map $g(x, y)$ to model a sulcus with cross-sectional width w mm, depth d mm, and length L, where L is chosen such that the sulcal sheet has a dimension of L^2 cm^2 (see Figure 2). The orientation $\eta(x, y)$ of the CSD at $g(x, y)$ is determined by the normal vector

$$\eta(x, y) = \frac{\partial g_x}{|\partial_x g|} \times \frac{\partial g_y}{|\partial_y g|},$$

where ∂g_x and ∂g_y are the tangent vectors at $g(x, y)$. Sulcal depths lie in the range 0 - 30 mm (van Essen, 2005) and sulcal widths typically do not exceed 10 mm (Kochunov et al., 2005). We choose nominal values of $w = 5$ mm and $d = 15$ mm, which gives a surface area of $L^2 \approx 9$ cm^2. The electrotonic space constant λ of the apical dendrites of neocortical pyramidal neurons is given by $\lambda = \sqrt{dR_m/4R_a}$, where d denotes the apical dendrites' diameter, R_m its specific membrane resistance, and R_a its specific intracellular resistance (Kandel et al., 2000), which gives a range for λ between 0.2 and 1 mm (Duan et al., 2003; Ledergerber and Larkum, 2010; Kasevich and Laberge, 2011). Model parameters are listed in Table 1.

Table 1: Volume-conductor parameters, their symbols, units, and nominal values.

Description	Symbol	Unit	Nominal value
cortex radius	r_1	cm	8.5
skull radius	r_2	cm	8.7
scalp radius	r_3	cm	9
cortical conductivity	σ_1	S/m	0.33
skull conductivity	σ_2	S/m	0.0041
scalp conductivity	σ_3	S/m	0.33

2.3 Calculation of scalp EEG

EEG signals were simulated by computing the scalp voltages $V(p,t)$ at the 3D-electrode locations of the international 10-20 system of electrode placement and by subsequently re-referencing to the average-montage. We denote $\mathrm{EEG}_k(t)$ for the average-reference EEG signal at the k-th electrode. The scalp voltage $V(p,t)$ at location p and time t is calculated using the quasi-static approximation of the Maxwell equations (Hamalainen et al., 1993) and by modeling cortical tissue, skull, and scalp by isotropically conducting spheres (Hallez et al., 2007). Thus, the boundaries between brain volume, skull, and scalp are modeled by spherical shells with radii r_1, r_2, and r_3, respectively, with conductivities σ_1, σ_2, and σ_3, respectively. They have all been measured and were taken from the literature (Zhang, 1995). Scalp voltages due to the CSD on the modeled sulcus were calculated by numerically integrating a truncated infinite series expansion of the scalp voltage due to a single dipole over the spatial extent of the sulcus (Zhang, 1995).

2.4 Extraction of wave-templates

We use the term *wave* to refer to a temporally-periodic spatial pattern and the term *oscillation* to refer to a temporally-periodic signal at a given location. This terminology reflects the view that a wave comprises a spatial continuum of oscillations. Let $V_{k\Delta t}$ denote the electrode-vector of bandpass filtered EEG signals at time $k\Delta t$. We thus assume that the signals are sampled with frequency $1/\Delta t$. To extract wave-activity, we select a reference electrode and determine the samples $k_1\Delta t, \cdots, k_N\Delta t$ for which the oscillations at the reference electrode have a local maximum (see Figure 3A and B). We then compute the average period $\bar{T}$ of the oscillations at the reference electrode, thus

$$\bar{T} = \Delta t \left\langle k_{n+1} - k_n \right\rangle_n ,$$

where the brackets $\langle\rangle_n$ denote averaging over n. Wave-activity is captured by the *wave-template* W with $M = \bar{T}/\Delta t$, which consists of a series of voltage maps $W_1, \cdots, W_M$, spanning the average period of the oscillations recorded at the reference electrode. Specifically, the m-th voltage map W_m is constructed by averaging the data over the samples $k_1, \cdots, k_N$, translated over j samples:

$$W_m = \left\langle V_{(k_n+(m-1))\Delta t} \right\rangle_n ,$$

as illustrated in Figure 3C. In addition to the extraction of wave-templates, we also compute *single-cycle waves* by selecting the data between samples $k_l\Delta t$ and $k_{l+1}\Delta t$ for $l = 1, \cdots, N-1$. Spatial correlations coefficients between single-cycle waves and the corresponding template will be used to assess the extent to which templates are representative for the propagation of single-cycle oscillations as well as to estimate the duration of single-cycle waves.

Figure 3D and 3E show two alternative ways of representing wave-templates. The template's voltages at the different electrodes is represented by ordering the corresponding voltage time-series according to the latency of their peaks, relative to the peak of the reference electrode. These

representations were obtained by extending the template periodically. In both figures, the electrodes are ordered from top to bottom by increasing latency. Thus, in Figure 3D, the signal at the bottom corresponds to the template's voltage at the reference electrode. The black dots in Figure 3E correspond to the latency-peaks of the template's voltages.

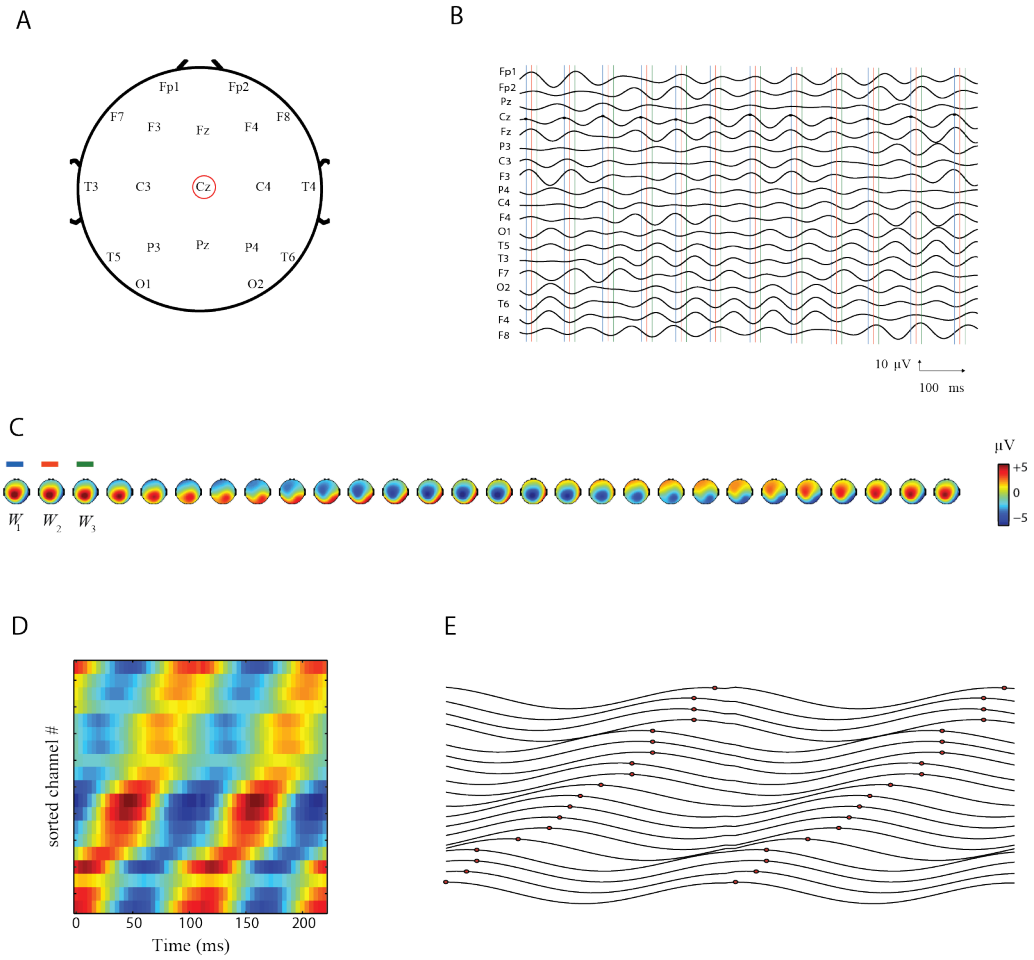

Figure 3: Extraction of wave templates. A. EEG electrode placement according to the international 10-20 system with corresponding electrode labels. In this example, the circled electrode Cz is chosen as reference electrode to extract the template. B. One-second epoch of EEG recording filtered in the alpha frequency band. The vertical bars denote the samples over which the time-series are averaged. The blue vertical lines are located at the samples n_i for which the signal at the reference electrode (Cz in this example) is locally maximal (black dots). The red and green lines are located at the shifted samples $n_i + 1$ and $n_i + 2$, respectively. C. Example of an extracted wave-template. The j-th voltage map of the template is obtained by averaging the EEG time-series over $n_i + j$, for $j = 1, \cdots, \bar{T}$, where $\bar{T} =< n_{i+1} - n_i >$ is the average period of the alpha oscillations. Note that the template is $\bar{T}$-periodic so that its duration equals the average alpha period. D and E. Two different ways of representating wave-templates. Both figures were obtained by sorting the time-series of the template according to the latency of their peaks, relative to the peak at the reference electrode. The black dots in E correspond to the peaks of the template's voltages.

2.5 Characterization of scalp waves

To characterize the propagation of a wave-template $W = W_1, \cdots, W_M$ we first compute its *positive and negative rectifications* W^+ and W^- by setting to zero all negative and positive values, respectively. Thus, the m-th voltage map of W^+ and W^- is given by $W_m^+ = W_m\Theta(W_m)$ and $W_m^- = W_m\Theta(-W_m)$, respectively, where Θ denotes the stepfunction, individually applied to the channels. This is illustrated in Figure 4A.

Next we compute the *positive and negative wave-centers* $\mu_m^+ = (\mu_m^+(x), \mu_m^+(y))$ and $\mu_m^- = (\mu_m^-(x), \mu_m^-(y))$ by weighting the electrode locations $c^x(k)$ and $c^y(k)$ by W_m^+ and W_m^-, respectively. Thus,

$$\mu_m^+(x) = \frac{1}{a_m} \left\langle W_m^+(k) c^x(k) \right\rangle_k ,$$

and

$$\mu_m^+(y) = \frac{1}{a_m} \left\langle W_m^+(k) c^y(k) \right\rangle_k ,$$

and similarly for μ_m^-, where k runs over the electrodes and a_m denotes the voltage of the m-th voltage map of W^+ summed over all electrodes. The normalization by a_m weighs the electrode locations by the voltage density, hence factors out global variations in EEG amplitude over time as well as over subjects. The quantities $\mu^+(x)$ and $\mu^+(y)$ track the center-of-mass of W^+ in the lateral and medial direction, respectively. Figure 4B provides an illustration. Instantaneous scalp velocities are estimated by finite differences between temporally consequtive wave-centers.

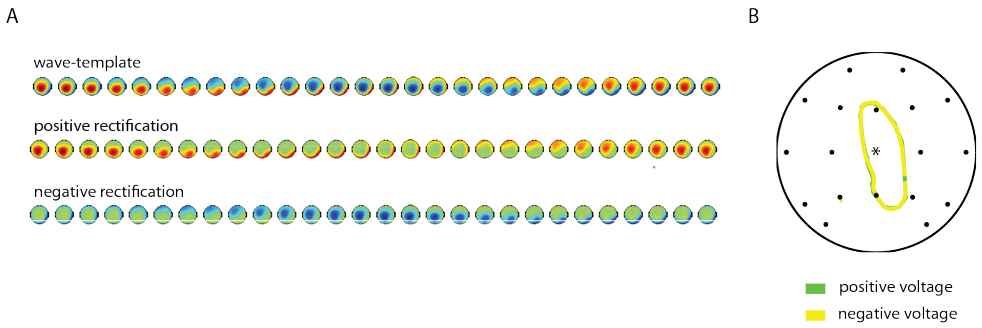

Figure 4: Rectified waves and scalp propagation. A. Example of a wave-template (first row) and the corresponding positively and negatively rectified templates (second and third row, respectively). B. Paths of the positive (green) and negative (yellow) wave-centers over the duration of the template. The star denotes the reference electrode that is used for constructing the wave template.

2.6 Predictions of the intra-cortical hypothesis

The expression for the scalp voltage $V(p,t)$ can be written in the following form:

$$V(p,t) = \frac{\lambda}{4\pi\sigma_3 r_3^2} \int\int \left\langle K\left(g(x,y),p\right), \eta_{x,y} s(x,y,t) \right\rangle dxdy,$$

for a certain kernel K, where $<,>$ denotes the inner-product, and where is integrated over the cortical square. That shows that $V(p,t)$ and hence EEG_k depend linearly on the CSD $\eta_{x,y}s(x,y,t)$ (Mosher et al., 1999). From this expression we can deduce that the following properties of the wave-centers μ_t^+ and μ_t^-. First, since $V(p,t+T) = V(p,t)$, where $T = 1/f$, it also holds that $\mathrm{EEG}_k(p,t+T) = \mathrm{EEG}_k(p,t)$, hence from the definition of μ_t^+ it follows that

$$\mu_{t+T}^+ = \mu_t^+,$$

and similarly for $\mu_{t+T}^- = \mu_t^-$. This means that the wave-centers are closed curves on the scalp with period T. Second, since $s(x,y,t+T/2) = -s(x,y,t)$, it holds that $\mathrm{EEG}_k(p,t+T/2) = -\mathrm{EEG}_k(p,t)$ and hence

$$\mu_{t+T/2}^+ = \mu_t^-.$$

This means that the positive and negative wave-centers are $T/2$ seconds out of phase. Note that since $V(p,t)$ is linear in both the electrotonic length-constant λ and CSD ηs, it follows that the wave-centers and hence their properties are independent of scalings in λ and ηs.

Third, the instantaneous speeds of the wave-centers are (approximately) symmetrically modulated over the period of the alpha oscillations. To see this, we approximate the oriented CSD $\eta_{x,y}s(x,y)$ by a rotating dipole with fixed location, we can show that the velocity of the maximum scalp voltage $V^{\max}(t)$ is symmetrically modulated in time over the period of the rotation. This property is only expected to hold approximately for the motion of μ_t^+ and only in certain cases, due to the dipole-approximation and because μ_t^+ concides with $V^{\max}(t)$ only in certain cases. Moreover, while $V^{\max}(t)$ traces out a circle for every period T, its projection on the 2D electrode locations can have a different shape.

Without loss of generality, we can assume that a dipole with unit-moment d_q is located at position $q = (|q|, 0)$, within the cortical shell ($|q| < r_1$) and rotates within the x-y-plane, thus $d_q = (\cos 2\pi ft, \sin 2\pi ft)$. We further assume that the resulting maximum scalp voltage $V^{\max}(t)$ traces out a circle with maximal radius r_3 (which could also be smaller, depending on the location and orientation of the dipole). We first calculate the location $p^{\max}(t)$ of $V^{\max}(t)$. Since $p^{\max}(t)$ lies on the line of the dipole moment d_q, there exists a scaling factor α_t such that

$$p^{\max}(t) = q + \alpha_t d_q.$$

Using the assumption that $|p^{\max}(t)| = r_3$, we can solve for α_t and obtain

$$\alpha_t = -|q| + \sqrt{\left(\cos^2\left(2\pi ft\right) - q\right)|q|^2 + r_3^2}.$$

The angle $\phi_p(t)$ of $p^{\max}(t)$ with the x-axis is now given by

$$\phi_p(t) = \tan^{-1}\left[\frac{\alpha_t \sin 2\pi ft}{|q| + \alpha_t \cos 2\pi ft}\right]$$

The speed $v_p(t)$ of $V^{\max}(t)$ in m/s is now given by

$$v_p(t) = 10^{-2} r_3 \frac{d\phi_p}{dt}(t).$$

Note that the average speed $\bar{v}_p = 10^{-2}\pi f r_3$ and that if the dipole lies at the origin, $v_p(t) = \bar{v}_p$. Thus, the modulation of scalp velocity is caused by the location on the dipole. For an alpha frequency of $f = 10$ Hz and scalp radius of $r_3 = 9$ cm, we get $\bar{v}_p \approx 5.7$ m/s. The symmetry of speed modulation is expressed as $\phi_p(T - t) = -\phi_p(t)$ which which follows directly.

Fourth, the average scalp velocity correlates both with alpha peak-frequency and with the spatial length of the wave-center curve. According to the intra-cortical hypothesis, the correlation between scalp speed and alpha peak-frequency is explained by the fact that, for fixed location and orientation of an activated sulcus, the wave-centers trace out the same curve over the duration of the alpha period. Furthermore, the correlation between scalp speed and curve length is explained by the fact that, for fixed alpha peak-frequency, variations in the traveling direction and locations of CSD waves on the cortex, the wave-centers trace out curves of different length but in equal times.

3 Results

3.1 Propagation of single-cycle oscillations

To assess if single alpha-cycles propagate over the scalp, we computed the single-cycle waves and computed the instantaneous velocities and averaged these over the waves and subsequently over subjects. The resulting velocity distribution is shown in Figure 5A. The average velocity is 2.26 ± 0.25 m/s. The narrow concentration around non-zero values demonstrates that single-cycle waves indeed propagate over the scalp. To assess if the wave-templates are representative for single-cycle waves, we computed the average spatial correlation coefficient of each single-cycle wave

with the corresponding template. The resulting histogram is shown in Figure 5B, which shows a strong bias towards high correlations. The average correlation coefficient is 0.58 ± 0.27.

To characterize the temporal correlations between single-cycle waves, we set the spatial correlation threshold to 0.8 and computed the number of succesive hits, where a single-cycle wave is considered a hit if its spatial correlation coefficient with the corresponding template exceeds the correlation threshold. The obtained numbers were averaged over subjects and the resulting distribution is shown in Figure 5C. The average number of sucessive hits is 2.90 ± 1.01 cycles. Note that although for the chosen correlation threshold, the average duration of single-cycle waves is in the order of hundreds of milliseconds, they can last up to 20 cycles, which is in the order of seconds.

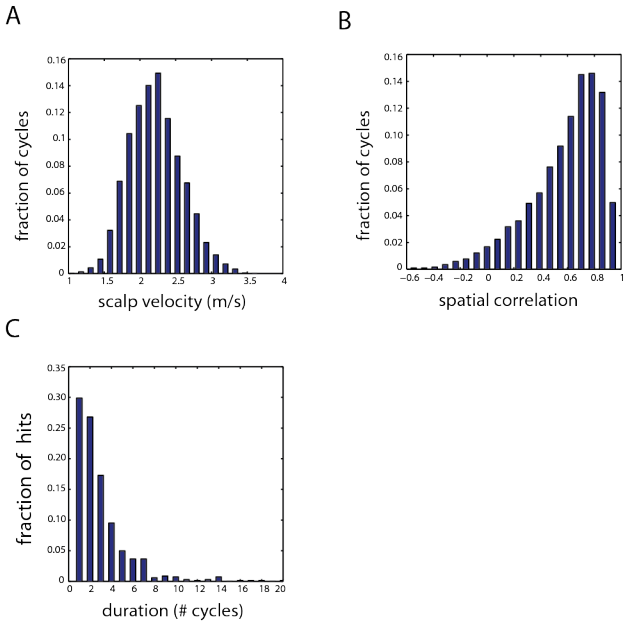

Figure 5: Propagation of sincle-cycle oscillations. A. Distribution of average scalp velocities. B. Distribution of spatial correlation coefficients between single-cycle waves and the corresponding templates. C. Distribution of durations of single-cycle waves, expressed in number of cycles. All distributions were obtained by pooling the data from all subjects.

3.2 Role of cortical convolutions

We first show that intra-cortically propagating alpha oscillations generate EEG potentials that lie in the right experimental range. The amplitudes at the electrodes that showed strongest alpha oscillations lie in the range 3 - 23 μV, with an average of 8.7 ± 4.2 μV. We set the model parameters to their nominal values (see Table 1) and varied the propagation velocity v and parallel length-constant λ_2 - which are the least experimentally restricted - in the range 0.1 - 1 m/s and 2 - 8 cm, respectively. For each combination of parameter values we simulated one oscillation period and computed the average-montage EEG signals at the sensor locations, and subsequently selected the sensor that had the highest amplitude. The resulting EEG voltages are shown in Figure 6A. The EEG voltages reach values up to about 6 μV. Combined with the uncertainty of maximal CSD values (100 - 250 μV) and membrane space-constants (0.2 - 6 mm), intra-cortically propagating alpha waves are able to generate EEG voltages up to about 16 μV, which agrees with the experementally observed values.

To assess how the CSD wave characteristics and cortical folding combine to give rise to strong EEG oscillations, we selected four pairs of parameter values (the numbered white dots in Figure 6A). For length constants that do not exceed about half the sulcal depth (15 mm in this case, see Table 1), only one sulcal wall is activated, which limits the total current density and thereby restricting scalp voltages to about 3 μV. This is illustrated in figure 6B, first image, which shows a snapshot of the cortical CSD and dipole moments for propagation speed and length constant set to 0.5 m/s and 2 cm, respectively. The moderate EEG voltage is generated by the aligned orientations of the dipole moments.

The case of slow propagation is shown is Figure 6B, second image, where propagation speed and length constant were set to 0.1 m/s and 10 cm, respectively. In this case, large EEG voltages

cannot by generated since due to slow propagation, wavelengths $\lambda = \nu/f_\alpha$ are short, leading to cancellation of oppositely oriented nearby dipole moments and hence to an attenuated electric field. On the other hand, fast propagation leads to simultaneous de- or hyperpolarization of opposite sulcal walls, as shown in figure 6B, third image, where propagation speed and length-constant were set to 1 m/s and 10 cm, respectively. Since dipole moments are now oriented in opposite directions, the electric field is attenuated, thereby restricting EEG voltages. Note that the propagation speeds for which this cancellation occurs depends on the depth of the sulcus, which illustrates the dependence of EEG voltages on the interplay between CSD dynamics and cortical folding.

Lastly, we set propagation speed and length-constant to 0.5 m/s and 10 cm, respectively, in which case one of the sulcal walls is depolarized and the other hyperpolarized, hence the dipole moments of both walls have the same orientation, thereby amplifying the electric field. We thus conclude that, given a fixed maximal CSD, the strongest EEG alpha oscillations are recorded when cortical wavelengths have about the same length as cortical convolutions.

Figure 6C shows two examples of simulated scalp waves. In both cases, propagation speed and length-constant were set to 0.5 m/s and 10 cm, respectively. The positions and locations of the sulci differ however, giving rise to qualitative different scalp dynamics. Scalp speeds were 2.0 m/s and 3.1 m/s, comparable with experimentally observed values (see Figure 5A). Also note the qualitative resemblance between the simulated scalp waves and the extracted EEG templates.

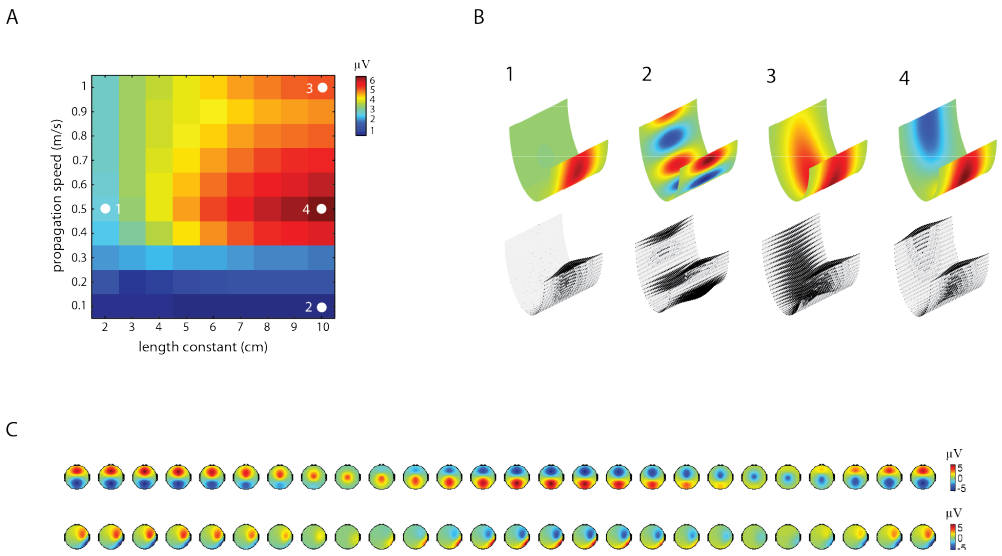

Figure 6: Effects of propagation velocity and spatial damping. A. Color-coded EEG voltages as a function of the propagation speed v and parallel length constant γ_2, which were varied in the range 0.1 - 1 m/s and 2 - 8 cm, respectively and in steps of 0.1 m/s and 1 cm, respectively. The numbered white dots correspond to the values 0.5 m/s and 2 cm, 0.1 m/s and 10 cm, 1 m/s and 10 cm, 0.5 m/s and 10 cm, respectively. B. Snapshots of the cortical CSD waves (top) and corresponding current dipoles (bottom) for the four chosen pairs of parameter values. C. Two examples of simulated scalp EEG waves.

3.3 Symmetric properties of scalp waves

The intra-cortical propagation hypothesis predicts that the centers of wave templates trace out closed curves on the scalp. To verify this, we computed the positive centers of the wave-templates of all subjects and calculated the mean distance between the center of the first and last voltage map. Averaged over subjects, the mean distance is 0.22 ± 0.16 cm. Comparing this value with the average curve-length, which is 27.2 ± 3.4 cm, the curves can reasonably be considered to be closed. Figure 7A shows the motion of the wave-center of a single subject.

The second prediction is that the positive and negative wave-centers lag exactly half the period of the wave-template, that is, half the average alpha period. To test this, we translated the negative wave-centers over half the template's period, computed the correlation coefficients between the original and translated lateral and medial coordinates, and subsequently averaged over the lateral and medial directions. The average correlation coefficient over all subjects is 0.96 ± 0.04, which comfirms this prediction. Figure 7B (top) shows the coordinates of the positive and negative wave-center of a single subject, where the negative wave-center has been translated over half the template's period.

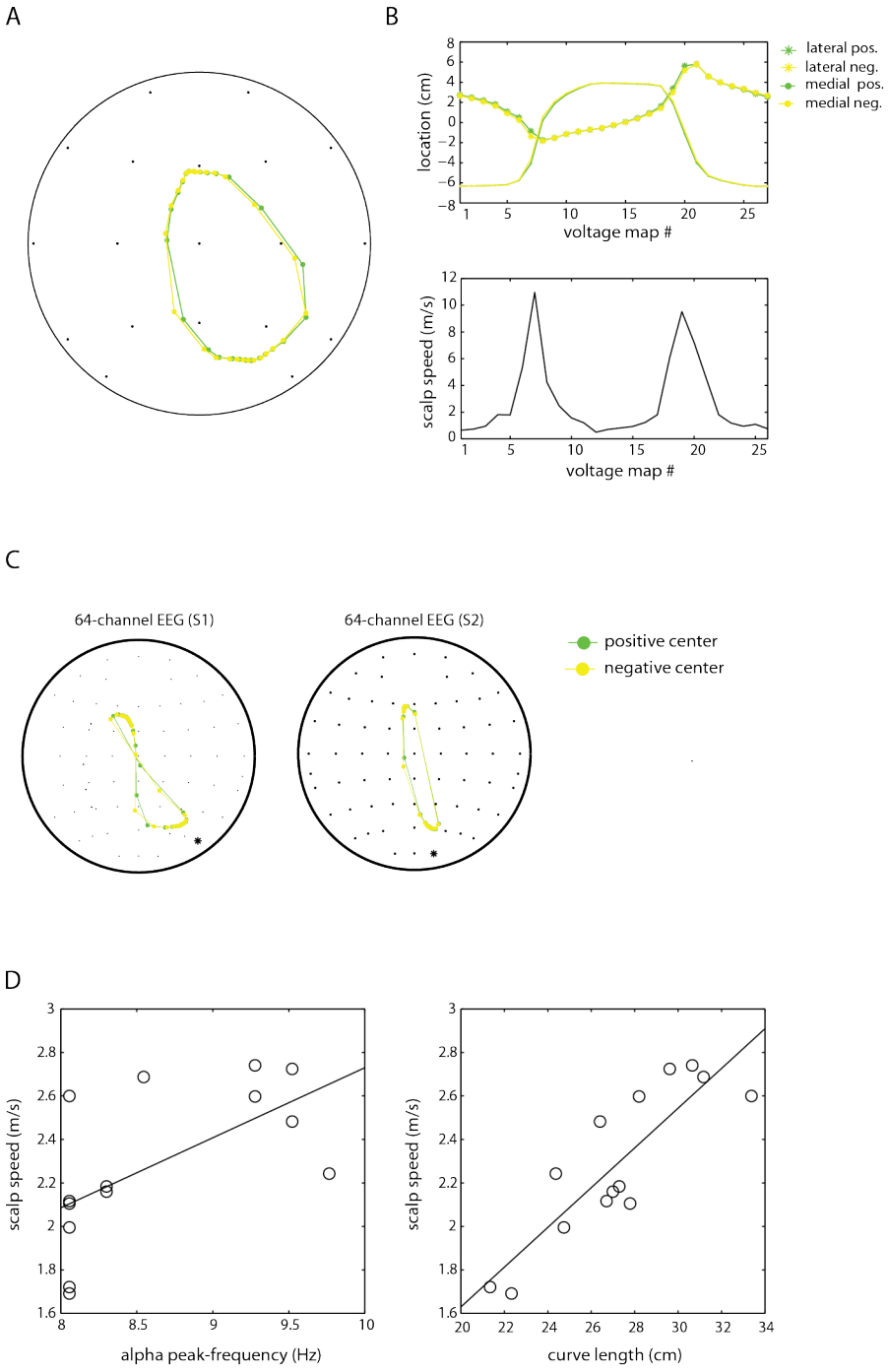

Figure 7: Verification of predictions of the intra-cortical propagation hypothesis. A. The closed curve traced out by the wave-center of a single subject (green: positive voltage, yellow: negative voltage). B. Top: traces of the medial and lateral coordinates of the positive wave-center (starred and dotted green lines, respectively) and the medial and lateral coordinates of the negative wave-center (starred and dotted yellow lines, respectively) translated over half the template's length. Bottom: Instantaneous scalp speed as a function of voltage map number. All examples correspond to the same subject. C. Motion of the wave-centers obtained from 64-channel EEG recordings in two subjects. The starts denote the reference electrodes for the construction of the wave-centers. D.

3.4 Modulation and correlates of scalp velocities

The third prediction that follows from the intra-cortical propagation hypothesis is that the instantaneous scalp velocities of the wave-centers are symmetrically modulated in time, that is, which a period equal to half the period of the corresponding template. To verify this prediction, we calculated the instantaneous velocities of all wave-centers and calculated the ratio of the number of voltage maps b etween the two highest maxima of the instantaneous velocity function with the number of voltage maps outside these maxima. Symmetric speed modulation is equivalent to a ratio of 0.5. We found an average ratio of 0.48 ± 0.02 which cannot be considered to be different from 0.5 at a 0.95%-confidence level ($p = 0.09$, two-sided sign test). Figure 7B (bottom) shows the instantaneous velocity for a single subject. Figure 7C shows the wave-centers that were obtained from 64-channel EEG recordings in two subjects. It can be seen that the curves traces out be the wave-centers are closed, that the positive and negative centers lag half the period of the alpha oscillation, and that the instantaneous velocities of the centers are symmetrically modulated just as above. This shows that the symmetry properties of the wave-centers are independent of the spatial sampling density of the scalp potential and in particular do not arise from a spatial undersampling of the scalp potential by the 10/20-electrode EEG system.

Lastly, the fourth prediction is that the average scalp velocity correlates both with alpha peak-frequency and with the spatial length of the wave-center curve. According to the intra-cortical hypothesis, the correlation between scalp speed and alpha peak-frequency is explained by the fact that, for fixed location and orientation of an activated sulcus, the wave-centers trace out the same curve over the duration of the alpha period. Furthermore, the correlation between scalp speed and curve length is explained by the fact that, for fixed alpha peak-frequency, variations in the traveling direction and locations of CSD waves on the cortex, the wave-centers trace out curves of different length but in equal times. We found correlations between alpha peak-frequency and

scalp velocity and between curve-length and scalp velocity of 0.61 ($p = 0.02$) and 0.86 ($p = 0.001$), respectively. The corresponding scatterplots are shown in Figure 7D.

4 Discussion

In this study we have shown that scalp EEG traveling waves can be accounted for by cortical oscillations that propagate through neocortical tissue with velocities in the range of propagation velocities of spikes in intra-cortical axons. Using different reference electrodes in the proposed analysis method biases the extraction of wave-activity to different cortical regions and it is expected that MEG recordings, which are less affected by the spatial blurring of electromagnetic fields (Hamalainen et al., 1993), allow the identification of a multitude of locally propagating alpha oscillations or "alphons" (Williamson et al., 1997) throughout neocortex. These findings thus challenge the view of spontaneous alpha oscillations as comprising a discrete network of local oscillators. Hence, conceptualizing the dynamics of spontaneous EEG or MEG oscillations in terms of functional networks (Pereda et al., 2005; Bullmore and Sporns, 2009) might not be the most natural. For instance, in our data, the lags between alpha oscillations recorded at different electrodes are all interrelated through a single traveling wave. In contrast to a description in terms of functional networks, this provides a more natural description that explains the interrelations between the lags. We suspect that in high-density EEG or MEG recordings, the combination of network-based methods and the extraction of traveling waves will provide a more comprehensive description of the dynamics of spontaneous oscillations than either method alone.

We employed biophysical modeling of the EEG to argue that the long-wavelength and fast propagating waves recorded from the scalp reflect spatially confined cortical oscillations that propagate through intra-cortical axons. Moreover, the properties of scalp waves are argued to be a direct

consequence of the local geometry and orientation of cortical convolutions. We do not claim that cortico-cortical axons do not play a role in shaping the large-scale dynamics of resting-state alpha oscillations. Indeed, a strong indication for such a role is provided by the reconstruction of the default-mode network from source-projected MEG alpha oscillations (Raichle et al., 2001; Brookes et al., 2011) and the resemblance between cortico-cortical white matter networks derived from diffusion tensor tractography (DTI) and resting-state blood-oxygen-level-dependent (BOLD) default-mode correlations (Hagmann et al., 2008). Our results do show, however, that the long-wavelength and fast traveling scalp waves can be explained completely in terms of intra-cortical propagation of cortical oscillations. A theoretical basis for the underlying physiology is developed in (van Rotterdam and Silva, 1982), although more recent theorical models of alpha oscillations predict different propagation behavior (Robinson et al., 1997; O'Connor and Robinson, 2004). A strategy to assess the contribution of cortico-cortical axons in coordinating locally propagating oscillations is to apply the presented analysis method to resting-state MEG recordings.

The notion of fast propagating cortical alpha oscillations (Burkitt et al., 2000; Nunez et al., 2001; Ito et al., 2005; Klimesch et al., 2007; Patten et al., 2012) derives from the identification of scalp propagation velocities and wavelengths with those in neocortex. For non-dispersive waves, wavelengths are given by $\lambda = v/f$, where v is the propagation velocity and f is alpha peak-frequency. Given the fact that frontal and occipital EEG alpha oscillations are anti-correlated, the identification of scalp waves with those on the cortex predicts a negative correlation between cortical surface area and alpha peak-frequency, for which there has been found no evidence (Valdés-hernández et al., 2010). This identification also leads to the notion that the anti-correlation between frontal and occipital scalp electrodes reflects long-wavelength standing waves in neocortex (Burkitt et al., 2000; Nunez et al., 2001; Ito et al., 2005). Although it has been hypothesized that cortical standing waves result from the superposition of waves traveling in opposite directions (Nunez et al., 2001), the

observed anti-correlation finds a simpler explanation as resulting from simultaneous measurements of opposite polarities of the electric field generated by a local cortical activations. Moreover, our study has shown that genuine standing scalp waves do not exist but are in fact propagating waves with a large modulation in propagation speed, resulting from the location and geometry of cortical convolutions.

The use of the proposed analysis method to extract wave-activity from EEG or MEG recordings provided evidence that single-cycle EEG alpha oscillations propagate over the scalp. This finding contrasts the results of earlier studies, which report propagation only in the fraction of cycles (Ito et al., 2005; Patten et al., 2012). The cause for the contrasting results is that these studies restrict propagation to linearly increasing phases-differences along one-dimensional chains of electrodes. As we have demonstrated however, scalp velocities are not constant but symmetrically modulated. Moreover, the volume-conductor model makes clear that propagation along a single dimension occurs only in the special case of cortical activations whose dipole moments are confined to vertical cross-sections of spherical cortex. Another finding in earlies studies is that propagation of resting-state alpha oscillations occurs in opposite directions in about 50% of the cases (Ito et al., 2005; Patten et al., 2012). This observation is explained by the fact that the wave-centers trace out closed curves on the scalp, where directional measures detect the first or the second half of the curve with about 50% ‘chance. Thus, apart from the special class of cortical activations described above, alpha scalp oscillations cannot be assigned a unique traveling direction. Therefore, when investigating wave propagation using EEG or MEG recordings, we suggest the use of a general analysis method that is not confined to subsets of electrodes/sensors and does not pose restrictions upon propagation properties.

The verification of several predictions that follow from the intra-cortical hypothesis of alpha prop-

agation suggests that the cortico-cortical hypothesis (Burkitt et al., 2000; Nunez et al., 2001; Ito et al., 2005; Klimesch et al., 2007) might be incorrect. In particular, it renders the existence of alpha waves with wavelengths in the order of several tens of centimeters unlikely. As a consequency, it casts doubt on the notion of top-down and bottom-up interactions between occipital and frontal networks through long-wavelength alpha waves (Burkitt et al., 2000; Ito et al., 2005; Patten et al., 2012). Moreover, our results suggest that the dominant traveling direction of alpha oscillations along the medial axis reflects the geometry and orientation of cortical convolutions, and as such, cannot directly be ascribed a functional role. Instead, our estimate of the spatial confinement of propagation to several centimeters suggests that the functional mechanisms of human alpha oscillations have a more local character. Based on the current study, we advocate a shift in viewpoint on the dynamical organization of human alpha oscillations from discrete networks of local oscillations to a continuum of locally propagating waves, possibly coordinated through cortico-cortical pathways.

Acknowledgments

GD was supported by the ERC Advanced Grant: DYSTRUCTURE (n. 295129), by the Spanish Research Project SAF2010-16085 and by the CONSOLIDER-INGENIO 2010 Program CSD2007-00012, and the FP7-ICT BrainScales. The authors declare no competing financial interests.

References

Bahramisharif A, van Gerven MAJ, Aarnoutse EJ, Mercier MR, Schwartz TH, Foxe JJ, Ramsey NF, Jensen O (2013) Propagating Neocortical Gamma Bursts Are Coordinated by Traveling Alpha Waves. *Journal of Neuroscience* 33:18849–18854.

Brookes M, Woolrich M, Luckhoo H, Price D, Hale J, Stephenson M, Barnes G, Smith S, Morris P (2011) Investigating the electrophysiological basis of resting state networks using magnetoencephalography. *Proceedings of the National Academy of Sciences* 108:16783–16788.

Bullmore E, Sporns O (2009) Complex brain networks : graph theoretical analysis of structural and functional systems. *Nature reviews. Neuroscience* 10:186–198.

Burkitt GR, Silberstein RB, Cadusch PJ, Wood AW (2000) Steady-state visual evoked potentials and travelling waves. *Clinical neurophysiology* 111:246–58.

Dijk HV, Schoffelen JM, Oostenveld R, Jensen O (2008) Prestimulus Oscillatory Activity in the Alpha Band Predicts Visual Discrimination Ability. *Journal of Neuroscience* 28:1816–1823.

Duan H, Wearne SL, Rocher AB, Macedo A, Morrison JH, Hof PR (2003) Age-related Dendritic and Spine Changes in Corticocortically Projecting Neurons in Macaque Monkeys. *Cerebral cortex (New York, N.Y. : 1991)* pp. 950–961.

Ermentrout GB, Kleinfeld D (2001) Traveling electrical waves in cortex: insights from phase dynamics and speculation on a computational role. *Neuron* 29:33–44.

Fellinger R, Gruber W, Zauner A, Freunberger R, Klimesch W (2012) Evoked traveling alpha waves predict visual-semantic categorization-speed. *NeuroImage* 59:3379–88.

Hagmann P, Cammoun L, Gigandet X, Meuli R, Honey CJ, Wedeen van J (2008) Mapping the Structural Core of Human Cerebral Cortex. *PLoS biology* 6.

Hallez H, Vanrumste B, Grech R, Muscat J, De Clercq W, Vergult A, D'Asseler Y, Camilleri KP, Fabri SG, Van Huffel S, Lemahieu I (2007) Review on solving the forward problem in EEG source analysis. *Journal of neuroengineering and rehabilitation* 4:46.

Hamalainen M, Hari R, Ilmoniemi RJ, Knuutila J, Lounasmaa OV (1993) Magnetoencephalographytheory, instrumentation, and applications to noninvasive studies of the working human brain. *Reviews Modern Physics* 65.

Han F, Caporale N, Dan Y (2008) Reverberation of recent visual experience in spontaneous cortical waves. *Neuron* 60:321–7.

Ito J, Nikolaev AR, van Leeuwen C (2005) Spatial and temporal structure of phase synchronization of spontaneous alpha EEG activity. *Biological cybernetics* 92:54–60.

Jensen O, Gelfand J, Kounios J, Lisman J (2002) Oscillations in the alpha band (9-12 Hz) increase with memory load during retention in a short-term memory task. *Cerebral cortex (New York, N.Y. : 1991)* 12:877–82.

Kandel E, Schwartz J, Jessell T (2000) *Principles of neuroscience.*

Kasevich RS, Laberge D (2011) Theory of Electric Resonance in the Neocortical Apical Dendrite. *PLoS ONE* 6.

Klimesch W (1999) EEG alpha and theta oscillations reflect cognitive and memory performance: a review and analysis. *Brain research. Brain research reviews* 29:169–95.

Klimesch W, Hanslmayr S, Sauseng P, Gruber WR, Doppelmayr M (2007) P1 and traveling alpha waves: evidence for evoked oscillations. *Journal of neurophysiology* 97:1311–8.

Kochunov P, Coyle T, Lancaster J, Thompson P, Rivie D, Cointepas Y, Re J, Schlosser A, Royall DR, Zilles K, Mazziotta J, Toga A, Fox PT (2005) Age-Related Morphology Trends of Cortical Sulci. *Human brain mapping* 26:210–220.

Ledergerber D, Larkum ME (2010) Properties of Layer 6 Pyramidal Neuron Apical Dendrites. *Journal of Neuroscience* 30:13031–13044.

Lopes Da Silva FH, Vos JE, Mooibroek J, van Rotterdam A (1980) Relative contributions of intracortial and thalamo-cortical processes in the generation of alpha rhythms, revealed by partial coherence analysis. *Electroencephalography* 50:449–456.

Makeig S, Westerfield M, Jung TP, Enghoff S, Townsend J, Courchesne E, Sejnowski TJ (2002) Dynamic brain sources of visual evoked responses. *Science (New York, N.Y.)* 295:690–4.

Mazaheri A, Jensen O (2008) Asymmetric Amplitude Modulations of Brain Oscillations Generate Slow Evoked Responses. *Journal of Neuroscience* 28:7781–7787.

Mo J, Schroeder CE, Ding M (2011) Attentional Modulation of Alpha Oscillations in Macaque Inferotemporal Cortex. *Journal of Neuroscience* 31:878–882.

Mosher JC, Leahy RM, Lewis PS (1999) EEG and MEG: forward solutions for inverse methods. *IEEE transactions on bio-medical engineering* 46:245–59.

Nikulin VV, Brismar T (2006) Phase synchronization between alpha and beta oscillations in the human electroencephalogram. *Neuroscience* 137:647–57.

Nunez PL, Wingeier BM, Silberstein RB (2001) Spatial-Temporal Structures of Human Alpha Rhythms : Theory , Microcurrent Sources , Multiscale Measurements , and Global Binding of Local Networks. *Human brain mapping* 164:125–164.

O'Connor SC, Robinson PA (2004) Unifying and interpreting the spectral wavenumber content of EEGs , ECoGs , and ERPs. *Journal of theoretical biology* 231:397–412.

Patten TM, Rennie CJ, Robinson PA, Gong P (2012) Human cortical traveling waves: dynamical properties and correlations with responses. *PloS one* 7:e38392.

Pereda E, Quiroga RQ, Bhattacharya J (2005) Nonlinear multivariate analysis of neurophysiological signals. *Progress in neurobiology* 77:1–37.

Raichle ME, Macleod AM, Snyder AZ, Powers WJ, Gusnard DA, Shulman GL (2001) A default mode of brain function. *Proceedings of the National Academy of Sciences* 98:676–682.

Robinson P, Rennie C, Wright J (1997) Propagation and stability of waves of electrical activity in the cerebral cortex. *Physical Review E* 56:826.

Valdés-hernández PA, Ojeda-gonzález A, Martínez-montes E, Lage-castellanos A, Virués-alba T, Valdés-urrutia L, Valdes-sosa PA (2010) White matter architecture rather than cortical surface area correlates with the EEG alpha rhythm. *NeuroImage* 49:2328–2339.

van Essen DC (2005) A population-average, landmark- and surface-based (PALS) atlas of human cerebral cortex. *NeuroImage* 28:635 – 662.

van Putten MJAM, Peters JM, Mulder SM, de Haas JM, Bruijninckx CMA, Tavy DLJ (2004) A brain symmetry index (BSI) for online EEG monitoring in carotid endarterectomy. *Clinical neurophysiology* 115:1189–94.

van Rotterdam A, Silva FLD (1982) A model of the spatial-temporal characteristics of the alpha rhythm. *Bulletin of Mathematical Biology* 44:283–305.

Williamson SJ, Kaufman L, Lu ZL, Wang JZ, Karron D (1997) Study of human alpha rhythm: the alphon hypothesis and alpha suppression. *International journal of psychophysiology* 26:63–76.

Wu JY, Xiaoying H., Chuan Z. (2008) Propagating waves of activity in the neocortex: what they are, what they do. *The Neuroscientist* 14:487–502.

Zhang Z (1995) A fast method to compute surface potentials generated by dipoles within multilayer anisotropic spheres. *Phys. Med. Biol.* 40:335–349.

Zheng L, Yao H (2012) Stimulus-entrained oscillatory activity propagates as waves from area 18 to 17 in cat visual cortex. *PloS one* 7:e41960.